physchem

MDPI

*Article*

# Exploring the Role of pH and Solar Light-Driven Decontamination with Singlet Oxygen in Removing Emerging Pollutants from Agri-Food Effluents: The Case of Acetamiprid

**Víctor Fabregat**

Department of Engineering and Innovation, Regenera Energy, C. Molina de Segura, 8, 30007 Murcia, Spain; vfabregat@regeneraenergy.es; Tel.: +34-69-3367-275

**Abstract:** Previously synthesized and tested water-dispersible photoactive polymeric microparticles have been employed as heterogenous photosensitizers to evaluate their performance in generating singlet oxygen through direct solar irradiation. This study utilizes these photocatalysts for the degradation of Acetamiprid in IWWTP wastewater effluents from the Agri-food industry, exploring, in addition to direct or simulated solar irradiation, the influence of pH on the photooxidation process. Over a thousand emerging pollutants, including pesticides like Acetamiprid, have been detected in aquatic environments in recent years, posing challenges due to the limitations of current wastewater treatment technologies. The developed method is particularly effective under basic or slightly basic conditions, aligning with the natural pH of wastewater and addressing a limitation of conventional Acetamiprid degradation methods, which typically require medium acidification to be effective. Polymers P3 and P4 exhibited high photocatalytic activity, achieving over 99% degradation of Acetamiprid through oxidation via singlet oxygen generated by Rose Bengal supported on the polymer matrix, while maintaining catalytic efficiency across multiple cycles. The results confirm that Acetamiprid removal from industrial wastewater via direct solar irradiation is feasible, though constrained by the availability of sufficient effective sunlight hours.

**Keywords:** photochemistry; solar photocatalytic treatment; industrial wastewater; singlet oxygen; emerging pollutants; acetamiprid; Rose Bengal



Academic Editor: Luísa Margarida Martins

Received: 2 December 2024
Revised: 1 February 2025
Accepted: 17 February 2025
Published: 22 February 2025

**Citation:** Fabregat, V. Exploring the Role of pH and Solar Light-Driven Decontamination with Singlet Oxygen in Removing Emerging Pollutants from Agri-Food Effluents: The Case of Acetamiprid. *Physchem* **2025**, *5*, 9. https://doi.org/10.3390/physchem5010009



## 1. Introduction

Photocatalysis provides a cost-effective and straightforward method for water purification, particularly in regions with abundant solar irradiation. However, its application is mostly limited to developing countries and is often associated with low levels of innovation [1–3]. In recent years, numerous studies have explored wastewater treatment through photocatalysis under visible light irradiation. Still, only a limited number have focused on the application of direct sunlight for this purpose. Of these, noteworthy studies have demonstrated the successful removal of emerging pollutants (EPs) from water using either direct sunlight or simulated solar irradiation [2–7].

The EPs, subsumed under the broader category of contaminants of emerging concern (CECs), encompasses an extensive array of substances including pharmacological agents, personal care products, endocrine-disrupting chemicals, and pesticides, as well as their metabolic byproducts, with over a thousand such entities documented within aquatic settings. A notable current challenge associated with EPs is the limitation of extant wastewater treatment technologies, such inefficacies contribute to the sustained presence of

EPs in aquatic ecosystems and in reclaimed waters utilized for irrigation purposes, thereby harboring potential repercussions for environmental integrity and public health [8–11]. In recent years, significant scientific efforts have focused on developing methods for the removal of emerging pollutants from water, either targeting specific compounds or entire pollutant groups. A variety of approaches have been explored, with many studies employing techniques such as adsorption and advanced oxidation processes, including photocatalysis, among other methods [11–19]. While many of these studies have been performed in laboratory settings, comprehensive studies have also investigated the elimination of EPs in real wastewater from wastewater treatment plants (WWTPs) or WWTPs processing industrial wastewater (IWWTPs) [20–24], including agri-food IWWTPs due to the hazards posed by EPs related to pesticides (insecticides, fungicides, etc.) [25–28].

In recent studies conducted by our research team on effluents from a IWWTPs of an agri-food sector company located in the Murcia Region (one of the leading agricultural regions in Europe for citrus and fresh vegetable production), recurrent traces of pesticides and fungicides have been identified [29–31]. While current regulations do not require the company to carry out such analyses to detect emerging pollutants, they occasionally choose to do so; as a general trend, glyphosate has been identified as the most widely used pesticide in the area. However, in recent years, other EPs, such as Acetamiprid, Imazalil, Thiabendazole, 2-Phenylphenol, Hexythiazox, Pyriproxyfen, Metalaxyl, or 2-amino-4-hydroxy-6-methyl–pyrimidine (AHMPD), have been increasingly detected. The potential prohibition of glyphosate may have led to an increase in the use of other families of pesticides [32]; however, in November 2023, the EU renewed the approval of the active substance glyphosate for 10 years.

(*E*)-N-(6-chloro-3-pyridylmethyl)-*N*′-cyano-*N*-methylacetamidine, known as Acetamiprid, is one of the identified pesticides that appears frequently throughout the year in the effluent analyses available. Acetamiprid is a neonicotinoid insecticide widely used on leafy vegetables, citrus, grapes, cherries, etc. [33–35]. Neonicotinoid pesticides have been used worldwide since the early 1990s; they exhibit high target efficacy, excellent physicochemical properties, and a wide spectrum of efficacy and low mammalian toxicity, making them strong candidates in future scenarios without glyphosate [32,35]. However, any chemical sprayed in fields will result in secondary effects on aquifers, biodiversity, and reclaimed water; this is also the case with Acetamiprid, which has been associated deleterious effects in honeybee queen production, increases in songbird mortality, or decreases in earthworm activity, and some studies even indicate toxicity in certain small mammals [33,34,36,37]. Moreover, their use in large quantities due to intensive agriculture and multiple cropping cycles per year can still be detrimental due to accumulation. This is particularly relevant in Spain, which leads in the use of pesticides within the European Union [38].

In recent years, the literature has documented significant research efforts aimed at the removal of Acetamiprid from wastewater via advanced oxidation methods [39]. Therefore, the photocatalytic degradation of Acetamiprid has been studied using inorganic photosensitizers, such as titanium dioxide ($TiO_2$) [40,41] or sulfate-doped $Ag_3PO_4$ with enhanced visible light activity [42]. However, the method that has yielded the best results is the photo-Fenton method, which is currently being extensively studied [43], even innovating in the materials used for metals used to catalyze hydroxyl (·OH) production, such as $\alpha$-$Fe_2O_3$-pillared bentonite/L-cysteine complex [44] or $NH_2$-MIL-88B(Fe) with different monodentate ligands in order to increase the pH action range [45]. Notably, the photo-Fenton method has been applied for wastewater treatment [46] and has also been combined with other methods such as ultrasound, enhancing its performance [47]. In sum, many concur that Acetamiprid is highly resistant to direct molecular ozone attack but its reaction with hydroxyl radicals exhibits fast kinetics [48]. The stringent acidic pH limitation is the

main barrier for Fenton implementation, taking into account that water and wastewaters effluents have a pH usually ranging between 6.5 and 8.5 [43].

An alternative that has not been extensively studied in the literature is the Acetamiprid oxidation via singlet oxygen ($O_2(^1\Delta_g)$), and that furthermore can solve the problem of application at basic medium. M.C. González determined in 2010 the reaction mechanism of Acetamiprid with $O_2(^1\Delta_g)$ using Rose Bengal (RB) as a photosensitizer [49]. RB is a xanthene-based natural compound that displays high absorption in the 500–600 nm range, its triplet state can be completely quenched by oxygen and so RB is considered a highly efficient photosensitizer for generating $O_2(^1\Delta_g)$ [50,51]. RB demonstrates a high quantum yield (ØΔ) of 0.75 for $O_2(^1\Delta_g)$ generation in water [52]; therefore, RB is widely used as photosensitizers for conducting singlet oxygen reactions in aqueous media. A notable advancement in recent years has been the application of Rose Bengal as a photosensitizer immobilized on organic polymers as heterogenous photocatalysts with highly effective approach for the treatment of contaminated effluents [53] or the degradation of EPs [54–57] under visible light irradiation. In fact, heterogenous photosensitizers with RB, which operate in the visible range, can address the major limitations of traditional photocatalysts like $TiO_2$, which are only active under UV radiation [58].

In this study, hydrophilic photoactive polymeric microparticles with covalently anchored RB were used as supported photosensitizers. The synthesis of these heterogeneous photocatalysts has been previously reported by our research group [59], as had their efficiency as photosensitizers in the evaluation of the repeated chemical transformations of a substrate through a mechanism involving chemical interaction and subsequent photocatalyst regeneration [59,60]. Recently, they have been successfully validated for the degradation of a fungicide by generating singlet oxygen under visible light irradiation, as demonstrated with AHMPD in real wastewater samples [31].

The objective of this research is to investigate the application of these photoactive materials for wastewater treatment through advanced oxidation processes involving singlet oxygen while evaluating the effect of pH and direct solar irradiation. The novelty of this study lies in the first-time investigation of Acetamiprid degradation via visible light photocatalysis using $O_2(^1\Delta_g)$ generated from supported RB photocatalysts and, additionally, to optimize physicochemical parameters, such as pH, to identify the optimal application range of the photoactive materials for Acetamiprid degradation. Their efficiency is evaluated under both laboratory conditions using simulated sunlight and natural sunlight in Murcia, one of the European regions with the highest solar irradiation. Previous results with AHMPD demonstrated the effectiveness of supported RB polymers [31], achieving high degradation rates in basic media despite slow kinetics; this study also aims to evaluate the kinetic $O_2(^1\Delta_g)$ performance of the photoactive materials for the degradation of Acetamiprid, an insecticide with a chemical structure distinct from AHMPD (a pyrimidine-based fungicide). The effectiveness of the photo-oxidation process will be compared to Fenton and photo-Fenton methods for Acetamiprid degradation, particularly in basic or slightly basic media. The application also will be studied both in laboratory samples and in real-scenario settings using effluent samples from an (IWWTP) in the agri-food sector.

## 2. Materials and Methods

### *2.1. Reactives and Materials*

Commercially solvents and reagents were used: Rose Bengal sodium salt (Fluka, Buchs, Switzerland), divinylbenzene (Fluka, Buchs, Switzerland, ~80% mixture of isomers), p-chloromethylstyrene (Sigma, Burlington, MA, USA, 90%), 2,2′-azobis(isobutyronitrile) (Sigma, Burlington, MA, USA, ≥98.0%), tetrabutylammonium hydroxide solution ~25% in methanol (~0.8 M) (Fluka, Buchs, Switzerland), γ-gluconolactone (Sigma, Burlington,

MA, US, ≥99%), ethylenediamine (Sigma, Burlington, MA, USA, ≥99%), Acetamiprid (Merck, Darmstadt, Germany), 9,10-anthracenedipropionic acid (Aldrich, Seelze, Germany, ≥98.0%), tetrahydrofuran (Scharlab, Barcelona, Spain, synthesis grade), 1-dodecanol (Aldrich, Seelze, Germany, 98%), ethyl acetate (Scharlab, Barcelona, Spain, synthesis grade), methanol (Scharlab, Barcelona, Spain, spectroscopy grade), ethanol (Scharlab, Barcelona, Spain, 96%), toluene (Scharlab, Barcelona, Spain, synthesis grade), 1,4-dioxane (Panreac, Darmstadt, Germany, spectroscopy grade), and N,N′-dimethylformamide (Aldrich, Seelze, Germany, treated previously with anhydrous $MgSO_4$).

### *2.2. Synthesis of the Photoactive Microparticles*

The polymeric photosensitizers employed in this study are derived from a method initially presented by D.C. Neckers where Rose Bengal was covalently attached to chloromethylated styrenic resins [61]. The hydrophilic properties of the synthesized materials are imparted through the incorporation of two hydrophilic functional groups—ethylenediamine and γ-gluconolactone—into the polymer matrix, following the approach outlined by J.M.J. Fréchet [62]. The experimental process for synthesizing the polymers is described below.

The synthesis of polymer P1 was conducted via a thermally initiated radical polymerization reaction. In a beaker, 100 mg of AIBN (1% by weight relative to the total weight) was dissolved along with a mixture of 6.67 g of divinylbenzene (DVB, isomer mixture, 80% grade) and 3.33 g of p-chloromethylstyrene (CME, 90% grade), maintaining a DVB/CME weight ratio of 2:1. The porogenic mixture, consisting of 12.50 g of 1-dodecanol (125% by weight of the polymerization mixture) and 2.50 g of toluene (25%), was then added to achieve a polymeric mixture/porogenic mixture ratio of 1:2. The resulting solution was homogenized and transferred into a glass tube, which was purged with nitrogen gas for 5 min. The tube was then sealed and placed in a silicone oil bath at 80 °C for 24 h, allowing the polymerization to proceed quantitatively. After this period, the system was cooled to room temperature, and the polymer was mechanically extracted from the mold. The resulting monolith was manually fragmented and placed into a cellulose extraction tube. It was washed with THF for 24 h at 85 °C using Soxhlet distillation to remove the porogenic mixture and any unreacted monomers or oligomers. Finally, the polymer was dried in a vacuum oven at 60 °C and ground into a fine white powder.

The second reaction step involved anchoring Rose Bengal onto the polymeric matrices obtained in the first step (P1). In a 500 mL two-neck round-bottom flask, 11.54 g of P1 (15 mmol of $–CH_2Cl$) and 17.62 g of Rose Bengal (17.32 mmol) were weighed. Subsequently, 400 mL of dry DMF was added, and the mixture was purged with nitrogen for 30 min. The reaction was conducted under reflux with stirring at 80 °C for 8 h. After cooling to room temperature, the solid polymer was filtered and sequentially washed with 200 mL portions of ethyl acetate, ethanol, 1:1 water/ethanol, water, 1:1 water/methanol, and methanol. Finally, the polymer was dried in a vacuum oven at 55 °C, yielding light pink polymeric particles. The process is shown in Figure 1.

To obtain polymer P3, P2 was reacted with ethylenediamine via a nucleophilic substitution $S_N2$ reaction [62], such that the ethylenediamine interacted with the chloromethyl groups that had not reacted in the previous step. A total of 9.33 g of P2 and 15 mL of ethylenediamine (in excess) were placed into a 250 mL two-neck round-bottom flask. The mixture was dispersed in 100 mL of dry THF, sealed, and purged with nitrogen for 30 min. The reaction mixture was then maintained under reflux at 70 °C for 8 h. After cooling to room temperature, the solid was filtered and washed sequentially with 200 mL portions of THF, dioxane, 1:1 dioxane/water, water, 1:1 dioxane/water, dioxane, and ethanol. Finally,

the polymer was dried in a vacuum oven at 55 °C, yielding polymeric particles with a brighter pink color compared to P2.

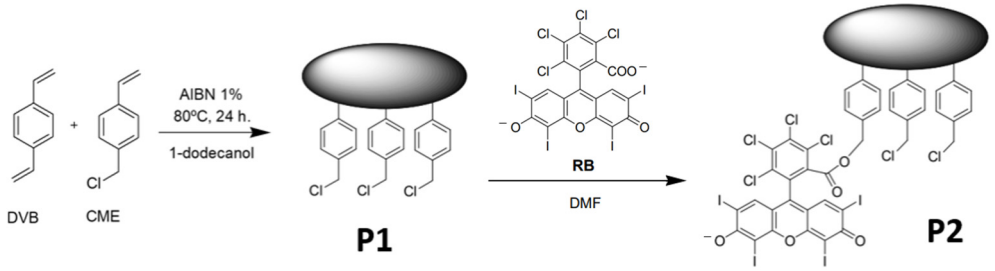


**Figure 1.** Chemical structure of polymers P1 and P2 along with their respective synthetic process.

Finally, to obtain the P4 polymer, a final reaction step was performed, involving the addition of γ-gluconolactone to the amine groups of the P3. In a 250 mL two-neck round-bottom flask, 5.74 g of P3 and 1.335 g of γ-gluconolactone (in excess) were introduced. The mixture was dispersed in 100 mL of absolute ethanol and purged with nitrogen for 30 min. The reaction was carried out under reflux at 80 °C for 18 h. After cooling to room temperature, the resulting polymer was filtered and sequentially washed with 200 mL portions of ethanol, 1:1 methanol/water, water, 1:1 methanol/water, and methanol. Finally, the obtained polymer (with a pink hue very similar to D3) was dried in a vacuum oven at 55 °C. The resulting P4 polymer exhibited a color very similar to that of P3 (Figure 2).

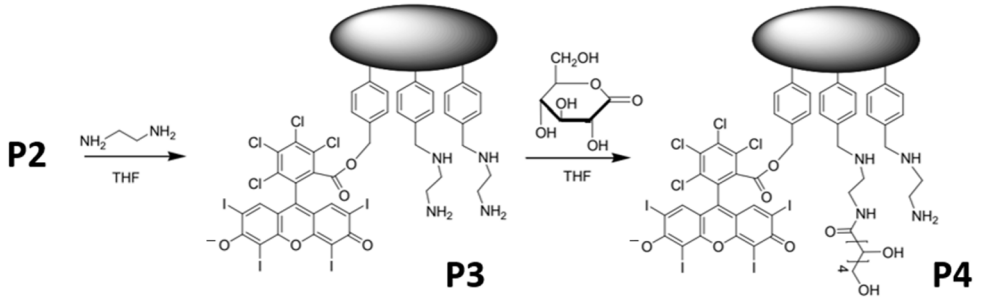


**Figure 2.** Chemical structure of polymers P3 and P4 along with their respective synthetic process.

*2.3. Characterization of the Microparticles*

The polymers are characterized in four stages. The first focuses on the polymerization process using FT-IR, FT-Raman spectroscopy, and thermogravimetric analysis (TGA). The second examines optical properties, including UV–Vis absorption, fluorescence spectroscopy, and particle size determination via granulometric analysis and SEM. FT-IR experiments were conducted using a JASCO FT/IR-6200 Type A instrument (JASCO Corporation, Tokio, Japan), while FT-Raman measurements were performed with a JASCO Laser Raman spectrometer (JASCO Corporation, Tokio, Japan). Thermal analyses were carried out with a Mettler Toledo TG-STDA instrument (Mettler Toledo, Greifensee, Switzerland), operating within a temperature range of 30–1000 °C at a heating rate of 5 °C/min in an air atmosphere. UV–Vis spectroscopic measurements were obtained using a Hewlett-Packard Agilent 8453 UV-Vis spectrometer (Agilent Technologies, Inc., Santa Clara, CA, USA), and fluorescence spectroscopy was performed with a Spex Fluorog 3-11 spectrofluorometer equipped with a 450 W xenon lamp (Horiba Scientific, Kioto, Japan), as the polychromatic light source. Particle size was performed using a JEOL 7001F SEM microscope (JEOL Ltd., Tokio, Japan), with polymeric samples coated in platinum.

In the third step, the RB content in the microparticles was determined by hydrolysis of RB-linked in the polymer matrix and its subsequent quantification using UV–Vis spec-

troscopy. To carry out this analysis, in a round-bottom flask, 40 mg of polymer, 1 mL of 1,4-dioxane, and 300 μL of a tetrabutylammonium hydroxide (TBAOH) solution in MeOH (0.8 M) were introduced. The flask was sealed and stirred at room temperature for 24 h. Afterward, the polymer was filtered and washed with MeOH. The filtrate was transferred to a 10 mL volumetric flask and brought to volume with MeOH. The determination of the amount of hydrolyzed RB was calculated by the Beer–Lambert law (λ = 557).

The final stage of the characterization involves assessing the ability of the materials to generate singlet oxygen. The singlet oxygen production capability of the materials was evaluated by analyzing the photo-oxidation kinetics of anthracene-9,10-dipropionic acid (ADPA) in Milli-Q water. For each polymer sample, 25 mg of the photosensitizer was mixed with 10 mL of an ADPA solution ($1.2 \times 10^{-4}$ M) in a test tube. The heterogeneous mixture was stirred and equilibrated with air. The test tubes were then exposed to irradiation at room temperature using a 50 W halogen lamp placed 2 cm from the samples. Control experiments, both in the dark and without a photosensitizer, were conducted to evaluate any potential adsorption of ADPA onto the polymeric photocatalyst. Additional controls for polymers P1–P4 were performed under the same conditions without a photosensitizer, involving only ADPA irradiation and the use of Rose Bengal (5 μM) as a reference photosensitizer. The progress of the ADPA photo-oxidation was monitored using UV–Vis spectrophotometry for 60 min by tracking the decrease in the ADPA absorption band at 398 nm. At each time interval, the reaction was paused by turning off the lamp, a 1 mL aliquot was taken to measure its absorption spectrum, and then returned to the reaction mixture before irradiation was resumed.

### *2.4. Kinetics of Acetamiprid Photo-Oxidation Using the Photoactive Microparticles*

The photo-oxidation rate of Acetamiprid was investigated using photosensitizers P2–P4 in aqueous solutions at a pH of 10. In each experiment, 25 mg of the photosensitizer was added to 10 mL of a 0.1 ppm Acetamiprid solution in a test tube. The heterogeneous mixture was stirred and equilibrated with air. The test tubes were irradiated at room temperature using a 125 W medium-pressure Hg vapor lamp, surrounded by an aqueous $FeCl_3$ solution (0.1 M) acting as a filter for wavelengths below 450 nm. The tubes were positioned 2 cm from the lamp. Control experiments were carried out in the dark to assess potential adsorption of Acetamiprid on the polymeric photocatalyst. Additional control tests were also conducted under the same conditions without any photosensitizer, and Rose Bengal (5 μM) was used as the photosensitizer. For kinetic studies at different pH values, each sample's pH was pre-adjusted accordingly by adding small quantities of 0.01 M HCl or 0.01 M NaOH. All experiments were performed in quintuplicate.

The method used to monitor Acetamiprid degradation involved pausing the reaction by turning off the lamp at each time interval, followed by collecting a 20 μL aliquot of the reaction mixture. The reaction was then resumed by switching the lamp back on to continue the process. The photo-oxidation reaction of Acetamiprid was determined by analyzing each aliquot by the HPLC chromatography ZORBAX column Reversed-Phase Agilent 1260 (Agilent Technologies, Inc., Santa Clara, CA, USA), using acetonitrile and water (1:2 volume ratio) as mobile phase, the Acetamiprid absorption was monitored at 243 nm with a flow rate of 1 $mL \cdot min^{-1}$ and a column temperature maintained at 30 °C.

### *2.5. Study of the Photocatalytic Pathway for Acetamiprid Photo-Oxidation*

The by-products identification was performed using GC-MS Shimadzu equipped with a quadrupole mass analyzer QP2010S (Shimadzu Corporation, Kyoto, Japan). A column Triazine Meta.X5 was employed, and the oven temperature was programmed to increase

from 60 °C to 240 °C at a rate of 6 °C per minute. Prior to the analysis, samples were concentrated and the organic compounds were eluted using 2 mL of methanol [49].

### *2.6. Studies of Acetamiprid Degradation with P3 and P4 Polymers as Photosensitizers in Industrial WWTP Samples*

To evaluate the degradation of Acetamiprid in wastewater, five effluent samples were collected from an industrial wastewater treatment plant (IWWTP) belonging to a Spanish agri-food company that specializes in citrus products. The company processes 40,000 tons of citrus annually, 90% being lemon-based products. It operates two lines—juices/concentrates and essential oils—consuming 20,000–30,000 $m^3$ of water yearly, 90% of which becomes wastewater. This wastewater is treated at the IWWTP to meet regulatory standards.

The photocatalytic experiments were conducted using the Hg vapor lamp, with each sample adjusted to pH = 10 to assess the reaction kinetics at this specific pH. The degradation of Acetamiprid during the photocatalytic process was monitored by HPLC chromatography at 243 nm, following the above-described experimental protocol. All experiments were performed in quintuplicate.

### *2.7. Reusability Studies with P3 and P4 Polymers in Acetamiprid Degradation*

Reusability experiments were conducted for polymers P3 and P4, using IWWTP water sample 1 adjusted at pH = 10 as the media and following the same procedure as previously described. The reaction time of each study was 300 min and cycle 2 was conducted without irradiation as a control. Ten reaction cycles were performed for each polymer.

### *2.8. Simulated and Direct Solar Irradiance Experiments*

The effect of solar irradiation from both 125 W mercury vapor lamp and real sunlight was analyzed. Initially, a study was conducted to determine the optimal irradiation distance for the simulated sunlight lamp. Up to this point, all experiments had been carried out at a fixed distance of 2 cm; however, for this study, the distance between the lamp and the test tube was systematically varied. The experiments were performed in quintuplicate using the P3 and P4 polymers, in combination with the $FeCl_3$ filter, and wastewater sample 5 from the IWWTP at pH = 10.

Subsequently, additional experiments were conducted with the P3 and P4 polymers under the same conditions as the simulated solar setup in the laboratory (wastewater sample 5, pH = 10, and $FeCl_3$ filter) but exposed to real sunlight on sunny days in Murcia during midday hours across different times of the year, to account for variations in solar irradiation. The solar irradiation incident on the surface of the reaction medium was measured using a Fluke IRR1-SOL meter (Fluke Europe B.V., Eindhoven, The Netherlands).

## 3. Results and Discussion

### *3.1. Synthesis and Characterization of the Photoactive Microparticles*

The synthesis and characterization of the photoactive microparticles were reproduced as described previously. The following are the results obtained from the characterization of each photoactive material. P1—FT-IR ($cm^{-1}$): 3018, 2917, 1629, 1425, 1265, 906, 795, 707. FT-Raman ($cm^{-1}$): 3058, 2906, 1631, 1408, 1267, 1181, 1001. The decomposition temperature is 500–510 °C, and the average particle diameter is 24.2 μm. P2—FT-IR ($cm^{-1}$): 3020, 2920, 1625, 1453, 1266, 902, 794, 709. FT-Raman ($cm^{-1}$): 3054, 2907, 1627, 1411, 1266, 1180, 1003. The decomposition temperature is 500–510 °C, UV–Vis absorption ($\lambda_{max}$, nm): 571, fluorescence emission ($\lambda_{max}$, nm): 602 ($\lambda_{ex}$ = 572 nm), Rose Bengal loading: 2 μmol RB $g^{-1}$ polymer, and the average particle diameter is 28.1 μm. P3—FT-IR ($cm^{-1}$): 3358, 3046, 2921, 1619, 1447, 990, 906, 798, 713. FT-Raman ($cm^{-1}$): 3055, 2903, 1632, 1407, 1315, 1179,

1105, 1003, 803. The decomposition temperature is 500–510 °C, UV–Vis absorption ($\lambda_{max}$, nm): 561, fluorescence emission ($\lambda_{max}$, nm): 593 ($\lambda_{ex}$ = 564 nm), Rose Bengal loading: 2 μmol RB $g^{-1}$ polymer, and the average particle diameter is 24.5 μm. P4—FT-IR ($cm^{-1}$): 3367, 3056, 2928, 1628, 1451, 1081, 902, 804, 704. FT-Raman ($cm^{-1}$): 3055, 2903, 1634, 1408, 1307, 1188, 1086, 1001, 930, 803. The decomposition temperature is 500–510 °C, UV–Vis absorption ($\lambda_{max}$, nm): 562, fluorescence emission ($\lambda_{max}$, nm): 591 ($\lambda_{ex}$ = 564 nm), Rose Bengal loading: 2 μmol RB $g^{-1}$ polymer, and the average particle diameter is 28.8 μm.

FT-IR and FT-Raman characterization results confirm successful polymerization across all polymers. For P3 and P4, broad bands between 3100 $cm^{-1}$ and 3600 $cm^{-1}$ are observed, corresponding to N-H stretching from ethylamine and O-H stretching from hydroxyl groups of γ-gluconolactone, respectively. Detailed spectra are provided in the Supplementary Materials. The amount of covalently anchored Rose Bengal in all polymers was determined to be 2 μmol of RB per gram of polymeric matrix, indicating that the addition reactions with ethylenediamine and γ-gluconolactone did not affect the covalently bound RB within the matrix. This value aligns with prior studies [31,59], as well as particle size measurements obtained through SEM microscopy. On the other hand, as shown in Figure 3, the polymeric matrices P2, P3, and P4 exhibit the characteristic pink color of Rose Bengal, with P3 and P4 showing slightly brighter shades than P2. UV–Vis absorption spectra confirm the presence of RB in all polymers, with absorption maxima between 562 nm and 571 nm, consistent with previous studies in the literature [31,59,63]. The polymers display broader spectral profiles and longer wavelength shifts compared to free RB ($\lambda_{max}$ = 557 nm), with P3 and P4 peaking at 561–562 nm and P2 at 571 nm. No leaching of RB was observed in any polymer when suspended in water.

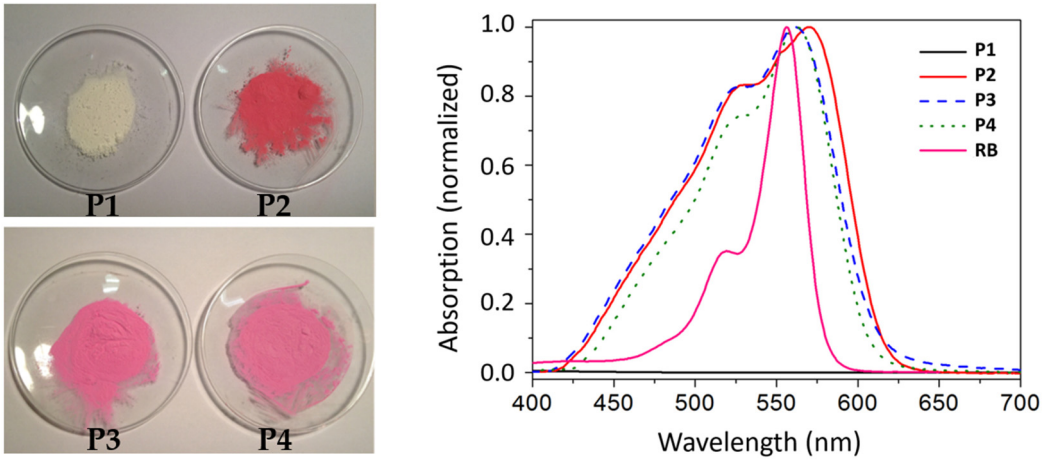


**Figure 3.** (**Left**): Illustration of the polymers P1, P2, P3, and P4. (**Right**): UV–Vis normalized absorption spectra for P1–P4 polymers (suspensions) and Rose Bengal (Milli-Q water, 5 μM).

P2–P4 polymers demonstrated photoactivity in terms of singlet oxygen generation. The characterization study was conducted by assessing the materials' ability to generate singlet oxygen, which was determined by analyzing the kinetics of the model reaction of photo-oxidation of anthracene-9,10-dipropionic acid to form ADPA-$O_2$ endoperoxide (60 min, 1.2 × $10^{-4}$ M of ADPA in Milli-Q water), which is widely studied in aqueous media. The results obtained are as follows: P1—maximum conversion: 0%. P2—maximum conversion: 85%; $K_{obs}$ ($min^{-1}$): 0.0432. P3—maximum conversion: >99%; $K_{obs}$ ($min^{-1}$): 0.0635. P4—maximum conversion: >99%; $K_{obs}$ ($min^{-1}$): 0.0640.

### 3.2. Study of the Kinetics of Acetamiprid Photo-Oxidation Using the Photoactive Microparticles

The effectiveness of polymers P1–P4 was evaluated in the photo-oxidation of Acetamiprid by monitoring the degradation of the pesticide, as described in Section 2.2 over time. The experiments were conducted at pH = 10 and control experiments carried out in the absence of light and without a photosensitizer, indicated no adsorption of Acetamiprid onto the polymers, nor any degradation of the compound through direct irradiation. The concentration of Acetamiprid was set at 0.1 ppm.

The degradation of Acetamiprid was monitored using HPLC chromatography; the traditional UV–Vis method employed in previous studies [31,59] cannot be applied in this case. Although the state of the art indicates that monitoring can also be carried out using 1H NMR and FTIR [40,41], the HPLC approach was selected due to it is the most widely used in the literature. Irradiation used the 125 W Hg vapor lamp with the 0.1 M $FeCl_3$ filter to block wavelengths below 450 nm, preventing Acetamiprid photolysis and Rose Bengal UV degradation.

The results obtained confirmed first-order kinetics in all cases for the degradation of Acetamiprid by singlet oxygen generated by Rose Bengal (Figure 4), as reported in the literature [49]. The kinetics of polymers P3 and P4, which are more hydrophilic, were superior to those of P2 and comparable to free RB. This confirms the successful incorporation of ethylenediamine and γ-gluconolactone through grafting into the polymeric matrix, enhancing the hydrophilicity of the microparticles; these results are consistent with prior research [31,59]. The values for the first-order kinetics are shown in Table 1, with the observed rate constants ($k_{obs}$) derived from fitting the conversion data over time. Additionally, the final conversion rates achieved for Rose Bengal and photosensitizers P2–P4 at pH = 10 are also reported. Conversions exceeding 99% were achieved with RB, P3, and P4 within a time frame of approximately 300 min (Figure 5).

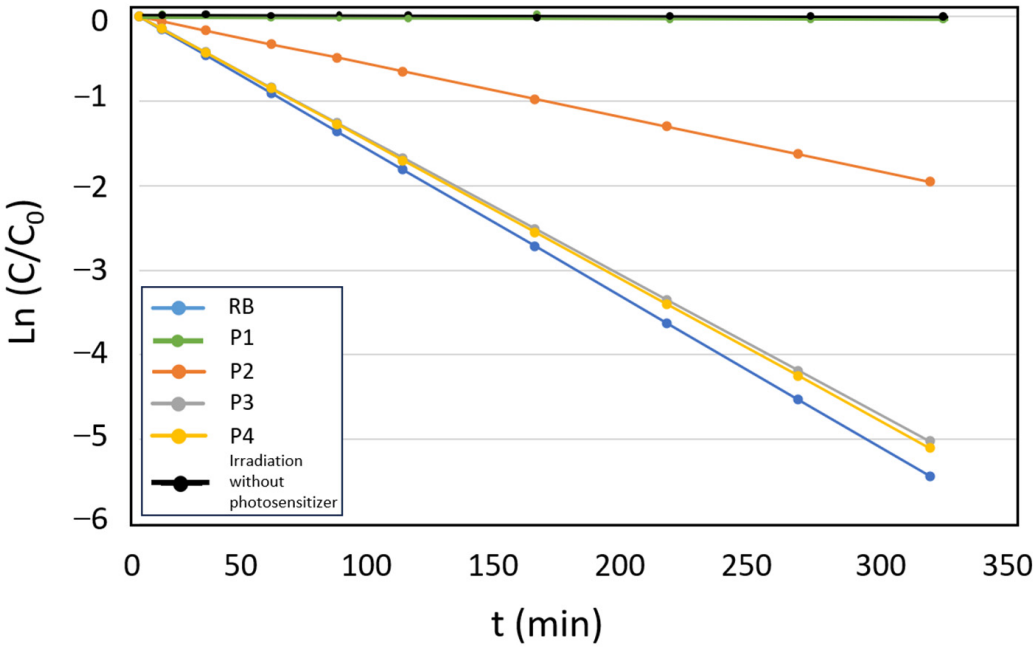


**Figure 4.** First-order kinetics of Acetamiprid photo-oxidation over time (C) relative to the initial concentration ($C_0$), for RB and P1–P4 (HPLC absorption maximum at 243 nm) at pH = 10.

**Table 1.** First-order constants and conversions for RB, P1, P2, P3, and P4 at pH = 10.

| Photosensitizer | | % Degradation | $K_{obs}$ ($min^{-1}$) |
|---|---|---|---|
| RB | Conversion (%)<br>t (min) | >99<br>305 | 0.0151 |
| P2 | Conversion (%)<br>t (min) | 85<br>350 | 0.0054 |
| P3 | Conversion (%)<br>t (min) | >99<br>330 | 0.0147 |
| P4 | Conversion (%)<br>t (min) | >99<br>325 | 0.0148 |

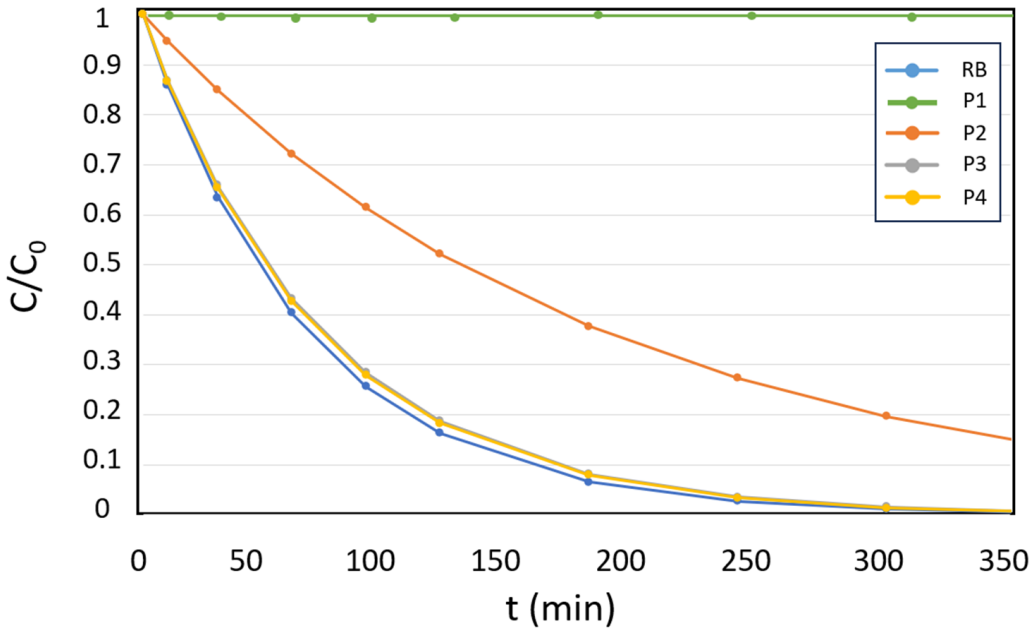


**Figure 5.** Degradation ratio of Acetamiprid over time (C) relative to the initial concentration ($C_0$), for RB and P1–P4 (HPLC absorption maximum at 243 nm) in pH = 10.

The influence of pH on the degradation kinetics of Acetamiprid was studied by assessing the Acetamiprid photo-oxidation in different pH scenarios. In this case, only polymers P3 and P4 were used, as they, as previously mentioned, exhibit higher performance than the nonpolar polymer P2. The effectiveness values of RB, P3, and P4 are presented in Table 2 in different pH reaction media.

Figure 6 compares the degradation rates of Acetamiprid at different pH values. As observed, Acetamiprid degradation is considerably more efficient in high pH media, achieving in all cases degradation rates of above 99% after 300 min of reaction for pH = 10 and higher and degradation rates of above 90% for pH = 8. The degradation of Acetamiprid is more effective under mildly basic or basic conditions, suggesting that the photo-oxidation mechanism is more efficiently promoted in alkaline conditions, as will be discussed in detail later.

**Table 2.** Conversions and first-order constants for RB, P3, and P4 in different pH media (t = 300 min).

| pH | Photosensitizer | % Degradation | $K_{obs}$ ($min^{-1}$) |
|---|---|---|---|
| 12 | RB | >99 | 0.0159 |
| | P3 | >99 | 0.0159 |
| | P4 | >99 | 0.0159 |
| 11 | RB | >99 | 0.0158 |
| | P3 | >99 | 0.0157 |
| | P4 | >99 | 0.0158 |
| 10 | RB | >99 | 0.0154 |
| | P3 | 98 | 0.0147 |
| | P4 | >99 | 0.0148 |
| 9 | RB | 98 | 0.0130 |
| | P3 | 96 | 0.0107 |
| | P4 | 96 | 0.0107 |
| 8 | RB | 92 | 0.0084 |
| | P3 | 90 | 0.0075 |
| | P4 | 90 | 0.0076 |
| 7 | RB | 85 | 0.0063 |
| | P3 | 82 | 0.0057 |
| | P4 | 83 | 0.0059 |
| 6 | RB | 72 | 0.0042 |
| | P3 | 68 | 0.0038 |
| | P4 | 68 | 0.0038 |
| 5 | RB | 53 | 0.0025 |
| | P3 | 50 | 0.0023 |
| | P4 | 50 | 0.0023 |

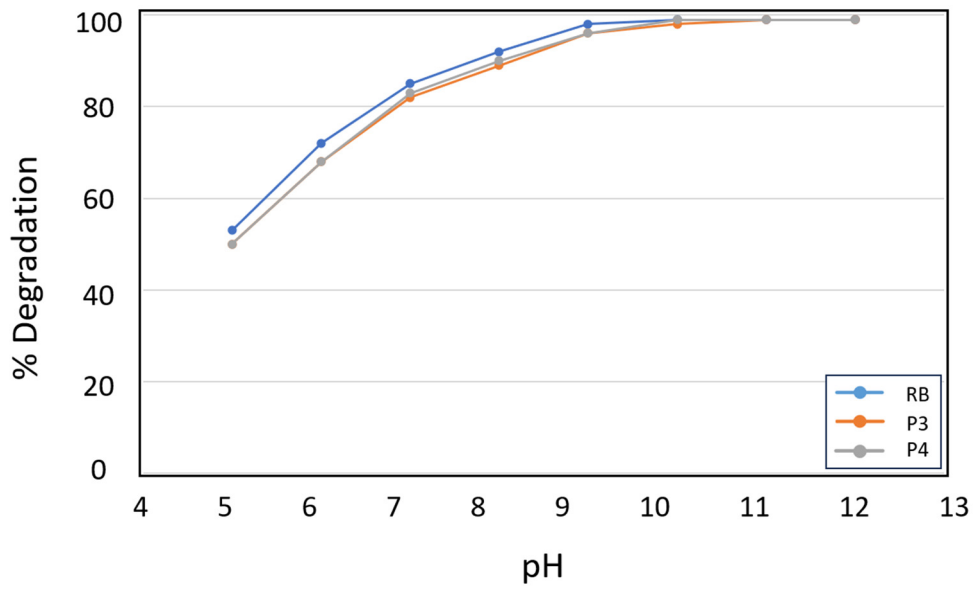


**Figure 6.** Degradation ratio of Acetamiprid for RB, P3, and P4 (t = 300 min) at different pH media.

### *3.3. Interpretation of the Photocatalytic Pathway for Acetamiprid Photo-Oxidation Using Rose Bengal as a Photosensitizer*

This section aims to explain the photo-oxidation mechanism of Acetamiprid via singlet oxygen using RB as a photosensitizer (whether supported or free-form). The first step of the mechanism is the Rose Bengal excitation: when the photosensitizer absorbs visible

light (500–600 nm), it transitions from its ground state to an excited singlet state (RB*) and singlet oxygen $O_2(^1\Delta_g)$ is generated from the ground state molecular oxygen $O_2(^3\sum_g)$. The subsequent interaction between singlet oxygen and Acetamiprid proceeds through a charge transfer mechanism, wherein $O_2(^1\Delta_g)$ acquires a partial negative charge while simultaneously inducing a partial positive charge on the Acetamiprid molecule. This observation aligns with the previously established literature, which interprets the mechanism of the photo-oxidation reaction of $O_2(^1\Delta_g)$ with substituted amines [64,65]. Gonzalez, who was the first researcher to investigate the photo-oxidation process of Acetamiprid using RB as a photosensitizer, supports this mechanism by indicating that the positive charge density is located on the nitrogen atom of the tertiary amine in the Acetamiprid and does not at the pyridine ring [49,66]. On the other hand, in a previous study, we reported that $O_2(^1\Delta_g)$ quenching increases the higher basicity of the solvent [31]. This is also suggested to occur in this reaction, where the positively charged form of Acetamiprid is favored as the pH becomes more basic, thereby enhancing the quenching with singlet oxygen (which possesses a negative charge density).

The literature reports that in the case of Acetamiprid, oxidation leads to the formation of various secondary amines (such as **b** in Figure 7) and aldehyde hydrates). Under strong oxidizing conditions, these aldehyde hydrates readily oxidize to their corresponding acids such as chloronicotinic acid (**a** in Figure 7) [43,45,49,67]. Furthermore, some authors demonstrate that the organic by-products from the degradation of Acetamiprid can ultimately be mineralized into purely inorganic compounds, such as carbon dioxide, water, nitric acid, and hydrochloric acid [40,45,48]. This is highly notable and aligns with the sustainability goals of total eliminating an organic emerging pollutant like the insecticide Acetamiprid in water.

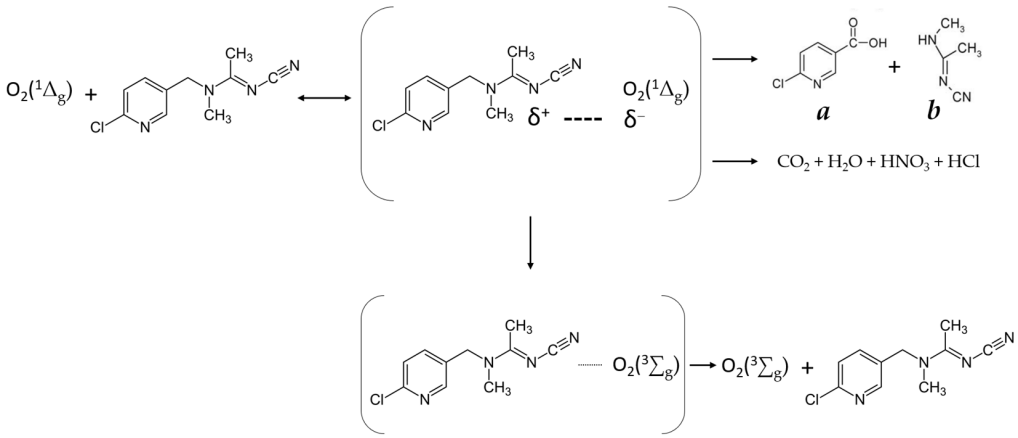


**Figure 7.** Quenching of singlet molecular oxygen $O_2(^1\Delta_g)$ by Acetamiprid. Compound **a** is chloronicotinic acid, and compound **b** is a secondary amine, both identified as oxidation products of Acetamiprid.

The by-products formed during the sensitized photo-oxidation of Acetamiprid were investigated with the aim of confirming the mechanism proposed for the reaction. The analysis was carried out using a GC-MS chromatography system equipped with a quadrupole mass analyzer. The results obtained have led to the identification of compounds **a** and **b**, as well as other by-products like aldehyde hydrates, such as formaldehyde and chloronicotinaldehyde, which have been previously reported in the literature [43,45,49]. Nevertheless, the decomposition into carbon dioxide, water, and nitric and hydrochloric acid was unable to be confirmed in this study.

On the other hand, the kinetics of both the ADPA and Acetamiprid experiments suggest that degradation is primarily driven by singlet oxygen photocatalysis, accord-

ing to the reaction kinetic patterns obtained [31,58]. Nevertheless, as supported by the literature, other reactive species, such as •OH radicals, may contribute to this process, particularly in the later stages of mineralization following degradation initiated by singlet oxygen activity [54,55,68]. However, the literature also indicates that organic photocatalysts are unlikely to produce hydroxyl radicals [53]. While the involvement of other reactive species cannot be entirely excluded, the reaction kinetics observed in this study strongly support singlet oxygen as the primary oxidizing agent. Additionally, hydroxyl radicals are known to acidify the reaction medium, a phenomenon that was not naturally observed in this investigation.

### *3.4. Acetamiprid Degradation Studies with P3–P4 Microparticles as Photosensitizers in Industrial WWTP Samples*

To evaluate the degradation potential of Acetamiprid in agri-food wastewater, five effluent samples from the IWWTP were analyzed. The pesticide concentrations in these samples were notably elevated, ranging between 0.045 ppm and 0.092 ppm, according to the analytical data provided by the IWWTP manager. The sample dates coincide with peak production periods for the agri-food company. Although current regulations do not require the company to perform such analyses to determine the presence of insecticides EPs, they conduct them occasionally. Consequently, the occurrence of high Acetamiprid concentrations in the IWWTP effluent, along with the underlying causes, remains unclear. This uncertainty is likely attributed to the pesticide's seasonal application on the citrus farms that supply the company. The photosensitizers P3 and P4 were utilized in the degradation tests of Acetamiprid using real water samples under two pH conditions: the actual pH of the sample and pre-adjusted at pH = 10. Table 3 presents the degradation results of Acetamiprid using P3 and P4 as photosensitizers under the two described pH conditions (reaction time of 360 min). The first-order kinetic constant obtained is also shown, along with the results for both controls: free RB and P1 (lacking RB in its structure).

**Table 3.** Acetamiprid degradation rates using P3 and P4 as photosensitizers in IWWTP samples.

| | | | **P3** | | **P4** | | **Control** | |
|---|---|---|---|---|---|---|---|---|
| **Sample** | **pH** | **[Acmp] ppm** | **% Deg (360 min)** | $k_{obs}$ **(min$^{-1}$)** | **% Deg (360 min)** | $k_{obs}$ **(min$^{-1}$)** | **% Deg (RB, 360 min)** | **% Deg (P1, 360 min)** |
| 1 | 7.8 | 0.045 | 92 | 0.0070 | 93 | 0.0074 | 93 | 0 |
| | 10 | | >99 | 0.0131 | >99 | 0.0138 | >99 | 0 |
| 2 | 7.7 | 0.053 | 91 | 0.0069 | 92 | 0.0072 | 93 | 0 |
| | 10 | | >99 | 0.0129 | >99 | 0.0132 | >99 | 0 |
| 3 | 7.8 | 0.068 | 90 | 0.0064 | 93 | 0.0075 | 94 | 0 |
| | 10 | | >99 | 0.0125 | >99 | 0.0139 | >99 | 0 |
| 4 | 7.6 | 0.079 | 93 | 0.0073 | 94 | 0.0077 | 94 | 0 |
| | 10 | | >99 | 0.0139 | >99 | 0.0145 | >99 | 0 |
| 5 | 7.8 | 0.092 | 92 | 0.0071 | 94 | 0.0079 | 95 | 0 |
| | 10 | | >99 | 0.0135 | >99 | 0.0147 | >99 | 0 |

The degradation rates observed in the industrial effluent samples closely align with the results obtained during the initial kinetic experiments at both pH = 7–8 and pH = 10 media, using P3 and P4 as photosensitizers. As expected, degradation was more effective at pH = 10 for all samples. It is significant to note that the monitoring of Acetamiprid degradation by HPLC did not show any interference, likely due to the possible presence of organic matter. Figure 8 presents a comparison of the Acetamiprid degradation rates over time

for effluent sample 1, utilizing the two polymeric photosensitizers P3 and P4, under both pH conditions.

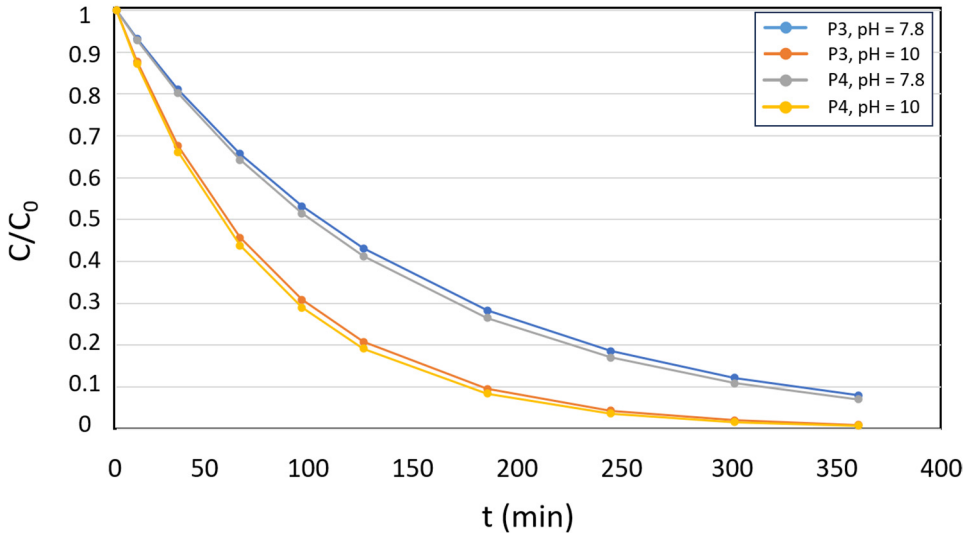


**Figure 8.** Degradation ratio of Acetamiprid over time (C) relative to the initial concentration ($C_0$), for effluent sample 1, with P3 and P4 as photosensitizers in pH conditions pre-adjusted to pH = 10 (measured in HPLC absorption maximum at 243 nm).

The results demonstrate that the supported photosensitizers can be effectively used for the degradation of Acetamiprid in effluent wastewater at its natural pH and more efficiently at pH = 10. In all cases, the degradation kinetics ranged from 300 to 360 min under such conditions. It is important to note that the proposed solution in this study addresses the limitations of traditional Fenton and photo-Fenton methods regarding their applicability at the effluent's natural pH. This also can minimize the risk associated with pH adjustments, where ions that can interfere with the reaction mechanism and affect the degradation rate of Acetamiprid [69,70].

Table 4 compares examples of different methods for the degradation of Acetamiprid, with the operational pH media and the kinetic times required to achieve complete degradation of the insecticide. The table provides examples of Fenton methods from key studies in the literature. In general, Fenton and photo-Fenton methods achieve Acetamiprid degradation rates exceeding 99% within approximately 1 h. These methods usually operate in a homogeneous medium and have been successfully applied on multiple occasions to wastewater treatment [43,46,67]. As discussed in the introduction section, the current state-of-the-art literature describes significant innovations in order to enhance efficiency of Fenton processes, particularly in terms of kinetics, achieving degradation within a few minutes. Additionally, some innovations have focused on expanding the pH operational range of the Fenton, such as the work by Zhao, which improved materials using monodentate ligands to extend the pH range of action [45], or Tabasum, who utilized graphene-oxide-based metal ferrites as Fenton-like as heterogeneous photocatalysts, successfully increasing the operational pH range [71].

The results obtained in this study should be compared with the examples described which apply the Fenton method at the natural pH of wastewater effluents, even with a higher degradation %. As outlined in the objectives, this work successfully describes an alternative to the Fenton and photo-Fenton methods for the removal of Acetamiprid at both the effluent pH and basic pH levels. Although this study demonstrates slower kinetics than the acidic pH Fenton method, the kinetics at a mildly basic pH are comparable in terms of time.

**Table 4.** Comparison of different Acetamiprid degradation techniques in different pH media.

| Method | Characteristics | % Degradation | t (min) | pH | Reference |
|---|---|---|---|---|---|
| $TiO_2$ | Heterogeneous | >99 | 1600 | 3 | [41,43] |
| Fenton | Homogeneous | >99 | 40 | 3 | [43,66] |
| Fenton | Homogeneous, wastewater | >99 | 90 | 3 | [43,66] |
| Photo-Fenton | Homogeneous | >99 | 10 | 2.8 | [43,72] |
| Photo-Fenton | Heterogeneous | >99 | 60 | 3 | [43,45] |
| Photo-Fenton | Heterogeneous | 78 | 240 | 9 | [43,45] |
| Fenton | Homogeneous, wastewater | >99 | 60 | 3 | [46] |
| Photo-Fenton | Homogeneous, wastewater | >99 | 30 | 3 | [46] |
| Fenton | Heterogeneous | >99 | 60 | 3 | [71] |
| Fenton | Heterogeneous | 30 | 60 | 8 | [71] |
| Singlet Oxygen | Heterogeneous, wastewater | 94 | 360 | 7.5–8 | This study |
| Singlet Oxygen | Heterogeneous, wastewater | >99 | 300 | 10 | |

### *3.5. Reusability Studies with P3 and P4 Polymers in Acetamiprid Degradation*

Recoverability experiments were conducted for polymers P3 and P4 using the IWWTP water sample 1. The samples were adjusted at pH = 10 and the time reaction was set at 300 min. This assay aims to determine the number of reaction cycles the polymeric photosensitizer can perform before experiencing any degradation. Cycle 2 was conducted without irradiation as a control. The results of the reusability experiments demonstrated that both heterogeneous photocatalysts, P3 and P4, retained over 99% conversion efficiency across ten catalytic cycles when tested for the photo-oxidative degradation of Acetamiprid. Additionally, the absence of leaching was verified by analyzing the absorption spectra of the corresponding supernatants following the second catalytic cycle. Figure 9 presents a time-based graph of cycles in which polymer P4 was used over 10 reaction cycles in the photo-oxidation of Acetamiprid without showing any degradation.

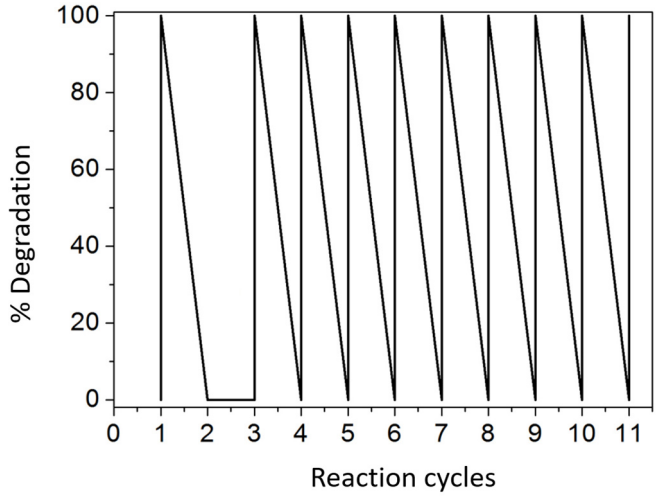


**Figure 9.** Scheme of the conversions achieved in successive reaction cycles of Acetamiprid photo-oxidation (IWWTP sample 1; pH = 10; reaction time per cycle = 300 min), using polymer P4 as the photosensitizer. Cycle 2 was conducted without irradiation.

### *3.6. Experimental Study with Simulated and Direct Solar Irradiance on IWWTP Samples*

After conducting optimization experiments to determine the optimal irradiation distance for the simulated sunlight lamp, the results indicate that a photocatalyst saturation effect occurs at a distance of less than approximately 8 cm from the light source. These

laboratory-scale experiments demonstrate that beyond this distance, an increase in the reaction time is required to achieve over 99% Acetamiprid removal.

As shown in Figure 10, when exceeding the photocatalyst saturation distance limit at approximately 8 cm, the reduced light intensity lowers the kinetic constant and drastically increases the time required to achieve more than 99% conversion of Acetamiprid. This suggests that the optimal distance for conducting experiments with simulated sunlight in the laboratory is less than 8 cm, where the full energy emitted by the lamp is effectively utilized. The results obtained for the reaction time as a function of distance fit well with a second-order polynomial regression model. The regression can be justified considering that the irradiance varies inversely with the square of the distance from the emitting source.

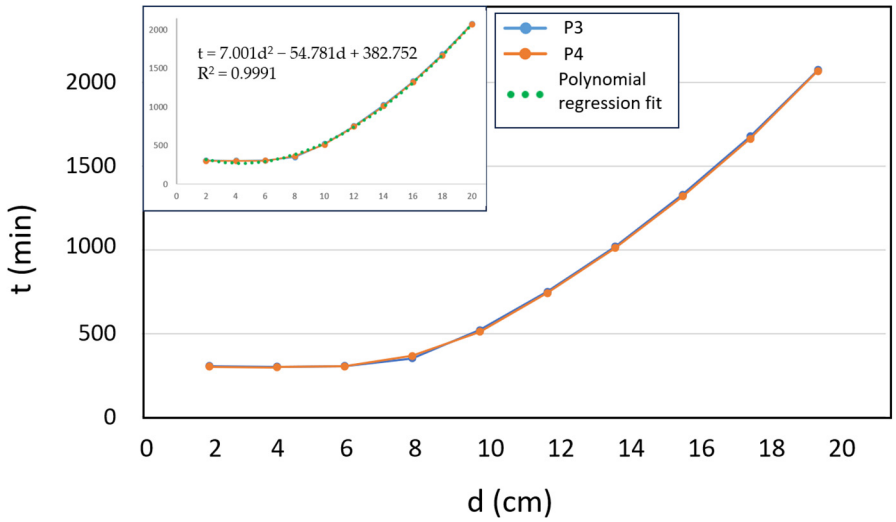


**Figure 10.** Effect of distance (d) on reaction time (t) for the >99% photocatalytic degradation of Acetamiprid using P3 and P4 (sample 5 of wastewater, pH = 10).

Regarding the experiments with direct solar irradiation, these were conducted similarly to those with simulated sunlight, using the P3 and P4 polymers, sample 5 of wastewater from the IWWTP at pH = 10, and the $FeCl_3$ filter. Table 5 presents the results of the photo-oxidation experiments of Acetamiprid conducted under solar irradiation during different times of the year in Murcia, with the average solar irradiation values recorded during the reaction time.

**Table 5.** Photocatalytic Acetamiprid degradation kinetic results under different solar irradiation values.

| Date | Solar Irradiation | Photosensitizer | Time to >99% Degradation | $K_{obs}$ ($min^{-1}$) |
|---|---|---|---|---|
| 27 June | 7.72 kWh/$m^2$ | P3 | 585 min | 0.007872 |
| | | P4 | 582 min | 0.007913 |
| 18 July | 7.33 kWh/$m^2$ | P3 | 614 min | 0.007494 |
| | | P4 | 613 min | 0.007513 |
| 8 August | 7.16 kWh/$m^2$ | P3 | 627 min | 0.007340 |
| | | P4 | 625 min | 0.007368 |
| 12 September | 6.49 kWh/$m^2$ | P3 | 678 min | 0.006790 |
| | | P4 | 677 min | 0.006802 |
| 17 October | 5.21 kWh/$m^2$ | P3 | 775 min | 0.005941 |
| | | P4 | 775 min | 0.005941 |
| 14 November | 3.35 kWh/$m^2$ | P3 | 916 min | 0.005027 |
| | | P4 | 915 min | 0.005033 |

The results obtained under Murcia's real sunlight, in the best-case scenario, with a degradation time of 585 min, correspond to an equivalent distance of 10.5 cm under simulated sunlight. Moreover, the solar irradiation experimental values are consistent with the historical average values of Murcia's solar irradiation, with an annual average of 5 $kWh/m^2/day$ [73]. During months with higher solar irradiation and extended daylight hours, such as from June to October, the daily sunlight duration is sufficient to achieve pesticide removal using the direct irradiation method, making the approach particularly effective during the summer.

On the other hand, it is important to note that while these distances are equivalent in terms of the kinetic values obtained in laboratory experiments under artificial sunlight and real sunlight, no direct equivalence can be established. It should be considered that the irradiation is different in each scenario due to the irradiated area on the test tube (illuminating only one side under artificial sunlight compared to all sides under direct sunlight). Additionally, for the 125 W mercury vapor lamp, only a small fraction of its power is emitted as usable light within the absorption range of RB. Furthermore, in both cases, the $FeCl_3$ filter is applied, blocking wavelengths below 450 nm, which further reduces the effective power, albeit with different components in each scenario.

Considering that in previous studies [31,59], these polymers were already optimized in terms of the ratio of RB incorporation into the polymer matrix and the amount introduced per reactor volume, the further improvement of the kinetic parameters under real sunlight conditions is not possible. This limitation stems from the inability to increase the amount of anchored RB photosensitizer to extend the kinetics. As a conclusion for real-world applications and as a continuation of previous studies, it can be determined that the removal of Acetamiprid from wastewater in industrial WWTPs is feasible, particularly during the summer and in months when the effective daylight hours with solar radiation intensity exceed Acetamiprid's degradation time, which occurs for approximately 7–8 months per year. Given that this method works, albeit with the limitation of the amount of photosensitizer per polymer weight, future work should focus on innovating the polymer matrix to achieve faster and more efficient kinetics under simulated and real sunlight conditions, while also ensuring compatibility with the pH range of wastewater plants. Additionally, further studies will explore the degradation of other pesticides compounds such as EPs.

## 4. Conclusions

Water-dispersible photoactive polymeric microparticles were employed in this study as heterogenous photocatalysts in the degradation of the pesticide Acetamiprid in IWWTP wastewater effluents. The designed polymers are active for the photocatalytic degradation of Acetamiprid under mildly basic and basic pH conditions. In all cases, employing polymers P2–P4 across various pH levels, both with laboratory samples and real effluent samples from IWWTP wastewater, the degradation kinetics of Acetamiprid exhibited first-order behavior. P3 and P4 materials allowed us to attain higher photochemical conversions than P2 materials, demonstrating that Acetamiprid degradation rates exceed 99% in basic media after 300 min of reaction and that degradation rates reach above 90–95% at the natural pH of wastewater effluents. The new polymers are capable of maintaining their catalytic activity for more than 10 cycles in an aqueous solution. The direct solar removal of Acetamiprid from industrial wastewater is feasible but constrained by the availability of effective sunlight hours, which is not sufficient during 4–5 months of the year. Future work should focus on optimizing the polymer matrix to enhance reaction kinetics under simulated sunlight conditions.

The kinetics observed in this study are slower than those described in the literature for traditional Fenton and photo-Fenton methods under acidic pH conditions. However, the successfully developed method describes an alternative to Fenton and photo-Fenton approaches for the removal of Acetamiprid at the effluent's natural pH, which is noteworthy as very high Acetamiprid removal rates are achieved. The photoactive materials demonstrate faster kinetics with the chemical structure of Acetamiprid than with the pyrimidine structure of AHMPD, as studied earlier. This comparison will provide insights into the general applicability and efficiency of RB-supported polymers in the degradation of various types of contaminants and other photo-transformations of environmental value. Further work will examine the use of the improved polymeric systems, as described herein, to evaluate their performance in the degradation of additional EPs structures; additionally, future research will explore the structural modifications of the polymeric materials to extend maximum efficiency to neutral pH and enhance the reaction kinetics in direct solar irradiation.

**Supplementary Materials:** The following supporting information can be downloaded at: https://www.mdpi.com/article/10.3390/physchem5010009/s1. Characterization data of P1–P4 microparticles: characterization of P1–P4 by thermogravimetric analysis: TGA P1–P4; legend: black curve represents the percentage of weight loss as a function of temperature, while the blue curve (TGA curve) indicates the percentage of weight loss over time, the red curve (DTG curve) displays the first derivative of the TGA curve, showing the rate of weight loss with respect to temperature; characterization of P1–P4 polymers by FT-Raman and FT-IR spectroscopy: spectroscopy P1, spectroscopy P2, spectroscopy P3, and spectroscopy P4; legend for FT-Raman: Raman intensity in arbitrary units as a function of frequency ($cm^{-1}$); legend for FT-IR: percentage transmittance (%T) as a function of frequency ($cm^{-1}$).

**Funding:** This research was funded by the Spanish Ministry of Science and Innovation through the State Investigation Agency via the Torres Quevedo industrial postdoctoral program PTQ2020-011517.

**Data Availability Statement:** Data are contained within the article.

**Acknowledgments:** The author wishes to express their gratitude to their PhD thesis supervisors at the Universitat Jaume I for their mentorship in the design of polymeric photoactive materials. Furthermore, the author extends their thanks to Regenera Energy for the opportunity to undertake an industrial postdoctoral fellowship and to the agri-food company that supplied the IWWTP samples (which has chosen to remain anonymous).

**Conflicts of Interest:** The author declares that the research was conducted in the absence of any commercial or financial relationships that could be construed as a potential conflict of interest.

## References

1. Alrousan, D.M.; Dunlop, P.S.; McMurray, T.A.; Byrne, J.A. Photocatalytic inactivation of E. coli in surface water using immobilised nanoparticle $TiO_2$ films. *Water Res.* **2009**, *43*, 47–54. [CrossRef] [PubMed]
2. Roy, J.S.; Messaddeq, Y. The Role of Solar Concentrators in Photocatalytic Wastewater Treatment. *Energies* **2024**, *17*, 4001. [CrossRef]
3. Villén, L.; Manjón, F.; García-Fresnadillo, D.; Orellana, G. Solar water disinfection by photocatalytic singlet oxygen production in heterogeneous medium. *Appl. Catal. B Environ.* **2006**, *69*, 1–9. [CrossRef]
4. Borges, M.E.; Sierra, M.; Cuevas, E.; García, R.D.; Esparza, P. Photocatalysis with solar energy: Sunlight-responsive photocatalyst based on $TiO_2$ loaded on a natural material for wastewater treatment. *Sol. Energy* **2016**, *135*, 527–535. [CrossRef]
5. Long, Z.; Li, Q.; Wei, T.; Zhang, G.; Ren, Z. Historical development and prospects of photocatalysts for pollutant removal in water. *J. Hazard. Mater.* **2020**, *395*, 122599. [CrossRef] [PubMed]
6. Saravanan, A.; Kumar, P.S.; Vo DV, N.; Yaashikaa, P.R.; Karishma, S.; Jeevanantham, S.; Bharathi, V.D. Photocatalysis for removal of environmental pollutants and fuel production: A review. *Environ. Chem. Lett.* **2021**, *19*, 441–463. [CrossRef]
7. Lee BC, Y.; Lim, F.Y.; Loh, W.H.; Ong, S.L.; Hu, J. Emerging contaminants: An overview of recent trends for their treatment and management using light-driven processes. *Water* **2021**, *13*, 2340. [CrossRef]

8. Morin-Crini, N.; Lichtfouse, E.; Liu, G.; Balaram, V.; Ribeiro, A.R.L.; Lu, Z.; Crini, G. Worldwide cases of water pollution by emerging contaminants: A review. *Environ. Chem. Lett.* **2022**, *20*, 2311–2338. [CrossRef]
9. Arman, N.Z.; Salmiati, S.; Aris, A.; Salim, M.R.; Nazifa, T.H.; Muhamad, M.S.; Marpongahtun, M. A review on emerging pollutants in the water environment: Existences, health effects and treatment processes. *Water* **2021**, *13*, 3258. [CrossRef]
10. Patel, N.A.V.E.E.N.; Khan, M.D.; Shahane, S.; Rai, D.; Chauhan, D.; Kant, C.; Chaudhary, V.K. Emerging pollutants in aquatic environment: Source, effect, and challenges in biomonitoring and bioremediation-a review. *Pollution* **2020**, *6*, 99–113.
11. Shahid, M.K.; Kashif, A.; Fuwad, A.; Choi, Y. Current advances in treatment technologies for removal of emerging contaminants from water–A critical review. *Coord. Chem. Rev.* **2021**, *442*, 213993. [CrossRef]
12. Pelosato, R.; Bolognino, I.; Fontana, F.; Sora, I.N. Applications of Heterogeneous Photocatalysis to the Degradation of Oxytetracycline in Water: A Review. *Molecules* **2022**, *27*, 2743. [CrossRef] [PubMed]
13. Madureira, J.; Melo, R.; Margaça, F.M.; Verde, S.C. Ionizing radiation for treatment of pharmaceutical compounds: A review. *J. Water Process Eng.* **2022**, *49*, 103179. [CrossRef]
14. Vasilachi, I.C.; Asiminicesei, D.M.; Fertu, D.I.; Gavrilescu, M. Occurrence and fate of emerging pollutants in water environment and options for their removal. *Water* **2021**, *13*, 181. [CrossRef]
15. Tijani, J.O.; Fatoba, O.O.; Madzivire, G.; Petrik, L.F. A review of combined advanced oxidation technologies for the removal of organic pollutants from water. *Water Air Soil Pollut.* **2014**, *225*, 1–30. [CrossRef]
16. Rathi, B.S.; Kumar, P.S.; Show, P.L. A review on effective removal of emerging contaminants from aquatic systems: Current trends and scope for further research. *J. Hazard. Mater.* **2021**, *409*, 124413. [CrossRef]
17. Lima, E.C. Removal of emerging contaminants from the environment by adsorption. *Ecotoxicol. Environ. Saf.* **2018**, *150*, 1–17.
18. Marin, M.L.; Santos-Juanes, L.; Arques, A.; Amat, A.M.; Miranda, M.A. Organic photocatalysts for the oxidation of pollutants and model compounds. *Chem. Rev.* **2012**, *112*, 1710–1750. [CrossRef] [PubMed]
19. Chatterjee, D.; Dasgupta, S. Visible light induced photocatalytic degradation of organic pollutants. *J. Photochem. Photobiol. C Photochem. Rev.* **2005**, *6*, 186–205. [CrossRef]
20. Bracamontes-Ruelas, A.R.; Reyes-Vidal, Y.; Irigoyen-Campuzano, J.R.; Reynoso-Cuevas, L. Simultaneous Oxidation of Emerging Pollutants in Real Wastewater by the Advanced Fenton Oxidation Process. *Catalysts* **2023**, *13*, 748. [CrossRef]
21. Vaiano, V.; De Marco, I. Removal of Azo Dyes from Wastewater through Heterogeneous Photocatalysis and Supercritical Water Oxidation. *Separations* **2023**, *10*, 230. [CrossRef]
22. Park, Y.; Kim, S.; Kim, J.; Khan, S.; Han, C. UV/$TiO_2$ Photocatalysis as an Efficient Livestock Wastewater Quaternary Treatment for Antibiotics Removal. *Water* **2022**, *14*, 958. [CrossRef]
23. Sodha, V.; Shahabuddin, S.; Gaur, R.; Ahmad, I.; Bandyopadhyay, R.; Sridewi, N. Comprehensive Review on Zeolite-Based Nanocomposites for Treatment of Effluents from Wastewater. *Nanomaterials* **2022**, *12*, 3199. [CrossRef]
24. Motamedi, M.; Yerushalmi, L.; Haghighat, F.; Chen, Z. Recent developments in photocatalysis of industrial effluents: A review and example of phenolic compounds degradation. *Chemosphere* **2022**, *296*, 133688. [CrossRef]
25. Madureira, J.; Margaça, F.M.; Santos-Buelga, C.; Ferreira, I.C.; Verde, S.C.; Barros, L. Applications of bioactive compounds extracted from olive industry wastes: A review. *Compr. Rev. Food Sci. Food Saf.* **2022**, *21*, 453–476. [CrossRef] [PubMed]
26. Madureira, J.; Barros, L.; Cabo Verde, S.; Margaça, F.M.; Santos-Buelga, C.; Ferreira, I.C. Ionizing radiation technologies to increase the extraction of bioactive compounds from agro-industrial residues: A review. *J. Agric. Food Chem.* **2020**, *68*, 11054–11067. [CrossRef]
27. Campos-Mañas, M.C.; Plaza-Bolaños, P.; Martínez-Piernas, A.B.; Sánchez-Pérez, J.A.; Agüera, A. Determination of pesticide levels in wastewater from an agro-food industry: Target, suspect and transformation product analysis. *Chemosphere* **2019**, *232*, 152–163. [CrossRef] [PubMed]
28. Jiménez-López, J.; Llorent-Martínez, E.J.; Ortega-Barrales, P.; Ruiz-Medina, A. Analysis of neonicotinoid pesticides in the agri-food sector: A critical assessment of the state of the art. *Appl. Spectrosc. Rev.* **2020**, *55*, 613–646. [CrossRef]
29. Life Clean Up. Available online: https://www.lifecleanup.eu/ (accessed on 13 November 2024).
30. Fabregat, V.; Pagán, J.M. Technical–Economic Feasibility of a New Method of Adsorbent Materials and Advanced Oxidation Techniques to Remove Emerging Pollutants in Treated Wastewater. *Water* **2024**, *16*, 814. [CrossRef]
31. Fabregat, V. Enhancing Emerging Pollutant Removal in Industrial Wastewater: Validation of a Photocatalysis Technology in Agri-Food Industry Effluents. *Appl. Sci.* **2024**, *14*, 6308. [CrossRef]
32. Mansfield, B.; Werner, M.; Berndt, C.; Shattuck, A.; Galt, R.; Williams, B.; Tittor, A. A new critical social science research agenda on pesticides. *Agric. Hum. Values* **2024**, *41*, 395–412. [CrossRef]
33. Potts, J. *Acetamiprid in the Environment: The Impact of Commercial Neonicotinoid Formulations on Soil Function and Ecology*; Bangor University: Gwynedd, UK, 2022.
34. Wallace, D.R. Acetamiprid. In *Encyclopedia of Toxicology*, 4th ed.; Elsevier: Amsterdam, The Netherlands, 2023; Volume 1–9, pp. V1–53.

35. Yamada, T.; Takahashi, H.; Hatano, R. A novel insecticide, acetamiprid. In *Nicotinoid Insecticides and the Nicotinic Acetylcholine Receptor*; Springer: Tokyo, Japan, 1999; pp. 149–176.
36. Zuščíková, L.; Bažány, D.; Greifová, H.; Knížatová, N.; Kováčik, A.; Lukáč, N.; Jambor, T. Screening of toxic effects of neonicotinoid insecticides with a focus on acetamiprid: A review. *Toxics* **2023**, *11*, 598. [CrossRef] [PubMed]
37. Phogat, A.; Singh, J.; Kumar, V.; Malik, V. Toxicity of the acetamiprid insecticide for mammals: A review. *Environ. Chem. Lett.* **2022**, *20*, 1453–1478. [CrossRef]
38. Le Basic. *EU Pesticides Export Ban: What Could Be the Consequences?* PAN EUROPE: Brussels, Belgium, 2024.
39. Yao, B.; Zhou, Y. Removal of neonicotinoid insecticides from water in various treatment processes: A review. *Crit. Rev. Environ. Sci. Technol.* **2024**, *54*, 1307–1339. [CrossRef]
40. Guzsvány, V.; Rajić, L.; Jović, B.; Orčić, D.; Csanádi, J.; Lazić, S.; Abramović, B. Spectroscopic monitoring of photocatalytic degradation of the insecticide acetamiprid and its degradation product 6-chloronicotinic acid on $TiO_2$ catalyst. *J. Environ. Sci. Health Part A* **2012**, *47*, 1919–1929. [CrossRef]
41. Zelić, I.E.; Povijač, K.; Gilja, V.; Tomašić, V.; Gomzi, Z. Photocatalytic degradation of acetamiprid in a rotating photoreactor-Determination of reactive species. *Catal. Commun.* **2022**, *169*, 106474. [CrossRef]
42. Lee, Y.J.; Kang, J.K.; Park, S.J.; Lee, C.G.; Moon, J.K.; Alvarez, P.J. Photocatalytic degradation of neonicotinoid insecticides using sulfate-doped Ag3PO4 with enhanced visible light activity. *Chem. Eng. J.* **2020**, *402*, 126183. [CrossRef]
43. Brillas, E. Fenton, photo-Fenton, electro-Fenton, and their combined treatments for the removal of insecticides from waters and soils. A review. *Sep. Purif. Technol.* **2022**, *284*, 120290. [CrossRef]
44. Song, Z.; Xu, Y.; Wu, H.; Huang, J.; Zhang, Y. Superior photo-Fenton degradation of acetamiprid by α-$Fe_2O_3$-pillared bentonite/L-cysteine complex: Synergy of L-cysteine and visible light. *J. Environ. Manag.* **2023**, *344*, 118523. [CrossRef] [PubMed]
45. Wang, Y.; Zhong, Z.; Muhammad, Y.; He, H.; Zhao, Z.; Nie, S.; Zhao, Z. Defect engineering of NH2-MIL-88B (Fe) using different monodentate ligands for enhancement of photo-Fenton catalytic performance of acetamiprid degradation. *Chem. Eng. J.* **2020**, *398*, 125684. [CrossRef]
46. Fasnabi, P.A.; Madhu, G.; Soloman, P.A. Removal of acetamiprid from wastewater by fenton and photo-fenton processes–optimization by response surface methodology and kinetics. *CLEAN–Soil Air Water* **2016**, *44*, 728–737. [CrossRef]
47. Patil, P.B.; Raut-Jadhav, S.; Topare, N.S.; Pandit, A.B. Combined strategy of hydrodynamic cavitation and Fenton chemistry for the intensified degradation of acetamiprid. *Sep. Purif. Technol.* **2023**, *325*, 124701. [CrossRef]
48. Cruz-Alcalde, A.; Sans, C.; Esplugas, S. Priority pesticides abatement by advanced water technologies: The case of acetamiprid removal by ozonation. *Sci. Total Environ.* **2017**, *599*, 1454–1461. [CrossRef] [PubMed]
49. Dell'Arciprete, M.L.; Santos-Juanes, L.; Arques, A.; Vercher, R.F.; Amat, A.M.; Furlong, J.P.; Gonzalez, M.C. Reactivity of neonicotinoid pesticides with singlet oxygen. *Catal. Today* **2010**, *151*, 137–142. [CrossRef]
50. Redmond, R.W.; Gamlin, J.N. A compilation of singlet oxygen yields from biologically relevant molecules. *Photochem. Photobiol.* **1999**, *70*, 391–475. [CrossRef] [PubMed]
51. Lambert, C.R.; Kochevar, I.E. Does rose bengal triplet generate superoxide anion? *J. Am. Chem. Soc.* **1996**, *118*, 3297–3298. [CrossRef]
52. Neckers, D.C. Rose Bengal. *J. Photochem. Photobiol. A Chem.* **1989**, *47*, 1–29. [CrossRef]
53. Blázquez-Moraleja, A.; Cabezuelo, O.; Martinez-Haya, R.; Schmidt, L.C.; Bosca, F.; Marin, M.L. Organic photoredox catalysts: Tuning the operating mechanisms in the degradation of pollutants. *Pure Appl. Chem.* **2023**, *95*, 899–912. [CrossRef]
54. Blázquez-Moraleja, A.; Moya, P.; Marin, M.L.; Bosca, F. Synthesis of novel heterogeneous photocatalysts based on Rose Bengal for effective wastewater disinfection and decontamination. *Catal. Today* **2023**, *413*, 113948. [CrossRef]
55. Flores, J.; Moya, P.; Bosca, F.; Marin, M.L. Photoreactivity of new rose bengal-$SiO_2$ heterogeneous photocatalysts with and without a magnetite core for drug degradation and disinfection. *Catal. Today* **2023**, *413*, 113994. [CrossRef]
56. Blázquez-Moraleja, A.; Bosio, A.; Gamba, S.; Bosca, F.; Marin, M.L. Covalent or ionic bonding of Eosin Y to silica: New visible-light photocatalysts for redox wastewater remediation. *J. Environ. Chem. Eng.* **2023**, *11*, 111024. [CrossRef]
57. Fabregat, V.; Pagán, J.M. A Green Chemistry and Energy Cost-Effective Approach in Innovative Advanced Oxidation Processes Through Photoactive Microgels for Sustainable Applications. *Preprints* **2025**, 2025012250. [CrossRef]
58. Li, J.; Liu, Y.; Zhu, Z.; Zhang, G.; Zou, T.; Zou, Z.; Xie, C. A full-sunlight-driven photocatalyst with super long-persistent energy storage ability. *Sci. Rep.* **2013**, *3*, 2409. [CrossRef] [PubMed]
59. Fabregat, V.; Burguete, M.I.; Galindo, F. Singlet oxygen generation by photoactive polymeric microparticles with enhanced aqueous compatibility. *Environ. Sci. Pollut. Res.* **2014**, *21*, 11884–11892. [CrossRef]
60. Fabregat, V.; Burguete, M.I.; Luis, S.V.; Galindo, F. Improving photocatalytic oxygenation mediated by polymer supported photosensitizers using semiconductor quantum dots as 'light antennas'. *RSC Adv.* **2017**, *7*, 35154–35158. [CrossRef]
61. Tamagaki, S.; Liesner, C.E.; Neckers, D.C. Polymer-based sensitizers for photochemical reactions. Silica gel as a support. *J. Org. Chem.* **1980**, *45*, 1573–1576. [CrossRef]

62. Wang, Q.C.; Svec, F.; Frechet, J.M. Hydrophilization of porous polystyrene-based continuous rod column. *Anal. Chem.* **1995**, *67*, 670–674. [CrossRef] [PubMed]
63. Paczkowska, B.; Paczkowski, J.; Neckers, D.C. Heterogeneous and semiheterogeneous photosensitization: Photochemical processes using derivatives of rose bengal. *Macromolecules* **1986**, *19*, 863–870. [CrossRef]
64. Young, R.H.; Martin, R.L.; Feriozi, D.; Brewer, D.; Kayser, R. On the mechanism of quenching of singlet oxygen by amines-iii. evidence for a charge-transfer-like complex. *Photochem. Photobiol.* **1973**, *17*, 233–244. [CrossRef]
65. Darmanyan, A.P.; Jenks, W.S.; Jardon, P. Charge-transfer quenching of singlet oxygen $O_2$ (1Δg) by amines and aromatic hydrocarbons. *J. Phys. Chem. A* **1998**, *102*, 7420–7426. [CrossRef]
66. Young, R.H.; Brewer, D. *Singlet Oxygen Reactions with Organic Compounds and Polymers*; Ranby, B., Rabek, J.F., Eds.; Wiley: Hoboken, NJ, USA, 1976; pp. 36–43.
67. Sirtori, C.; Agüera, A.; Carra, I.; Sanchéz Pérez, J.A. Application of liquid chromatography quadrupole time-of-flight mass spectrometry to the identification of acetamiprid transformation products generated under oxidative processes in different water matrices. *Anal. Bioanal. Chem.* **2014**, *406*, 2549–2558. [CrossRef] [PubMed]
68. Martínez-Haya, R.; Miranda, M.A.; Marin, M.L. Type I vs Type II photodegradation of pollutants. *Catal. Today* **2018**, *313*, 161–166. [CrossRef]
69. Pinto, M.I.; Salgado, R.; Laia CA, T.; Cooper, W.J.; Sontag, G.; Burrows, H.D.; Noronha, J.P. The effect of chloride ions and organic matter on the photodegradation of acetamiprid in saline waters. *J. Photochem. Photobiol. A Chem.* **2018**, *360*, 117–124. [CrossRef]
70. Rivas Ibáñez, G.; Casas López, J.L.; Esteban García, B.; Sánchez Pérez, J.A. Controlling pH in biological depuration of industrial wastewater to enable micropollutant removal using a further advanced oxidation process. *J. Chem. Technol. Biotechnol.* **2014**, *89*, 1274–1282. [CrossRef]
71. Tabasum, A.; Bhatti, I.A.; Nadeem, N.; Zahid, M.; Rehan, Z.A.; Hussain, T.; Jilani, A. Degradation of acetamiprid using graphene-oxide-based metal (Mn and Ni) ferrites as Fenton-like photocatalysts. *Water Sci. Technol.* **2020**, *81*, 178–189. [CrossRef]
72. Zbiljić, J.; Guzsvány, V.; Vajdle, O.; Prlina, B.; Agbaba, J.; Dalmacija, B.; Kalcher, K. Determination of $H_2O_2$ by $MnO_2$ modified screen printed carbon electrode during Fenton and visible light-assisted photo-Fenton based removal of acetamiprid from water. *J. Electroanal. Chem.* **2015**, *755*, 77–86. [CrossRef]
73. Available online: https://www.aemet.es/es/serviciosclimaticos/datosclimatologicos/atlas_radiacion_solar (accessed on 19 November 2024).